(This is a sample cover image for this issue. The actual cover is not yet available at this time.)

Deep-Sea Research I 58 (2011) 979–987

Contents lists available at ScienceDirect

Deep-Sea Research I

journal homepage: www.elsevier.com/locate/dsri

Dominant spatial variability scales from observations around the Hawaiian Islands

Dax Matthews[a,*], Brian Powell[a], Ralph Milliff[b]

[a] School of Ocean and Earth Science and Technology, University of Hawai'i, Manoa, USA
[b] Colorado Research Associates, NorthWest Research Associates, Inc., Boulder, Colorado, USA

ARTICLE INFO

Article history:
Received 23 March 2011
Received in revised form
3 July 2011
Accepted 25 July 2011
Available online 9 August 2011

Keywords:
Length scales
Mesoscale variability
Hawaiian Islands

ABSTRACT

We utilize a variety of available observations with a semivariogram technique to quantify the oceanic variability around the Hawaiian Islands. The Hawaiian Islands have a significant impact on the North Pacific circulation, and quantifying the characteristics of the variability is important for understanding the eddy energy, as well as required for statistical techniques to work with the data, such as optimal interpolation, data assimilation, etc. Both satellite sea surface height and temperature data are used to determine horizontal scales of variability, while Argo profiles, ship-borne profiles, and autonomous Seagliders provide estimates of the vertical scales. In the lee of the islands, satellite data reveal an increase in horizontal variability attributed to enhanced eddy activity that persists for over 1000 km westward; however, only within 400 km of the immediate lee the horizontal length scales are greatly reduced. Further west, length scales increase significantly indicating a change in the generation mechanism for eddy variability and where eddies merge and coalesce. The meridional length scale gradient is found to be larger than previous results and more representative of the gradient of the first baroclinic mode of the internal Rossby radius. Vertical length scales are shown to increase in the lee, with vertical temperature variability doubled from the windward side.

1. Introduction

Ocean dynamics occur over a wide range of time and space scales. Interannual and planetary dynamics occur at the largest scales, while smaller motions include local tides, surface waves, and ocean mixing. In general, the ocean is dominated by mesoscale fluctuations on time scales between 20 and 150 days and spatial scales between 50 and 500 km (Wyrtki et al., 1976; Danztler, 1977; Richman et al., 1977) that decrease poleward from the tropics (Mercier and Colin de Verdiere, 1985; Lee and Niiler, 1987). Applying autocorrelation to very advanced high-resolution radiometer (AVHRR) infrared data, Krause et al. (1990) estimated eddy scales in the North Atlantic that matched the Rossby radius of the first baroclinic mode. Similarly, Stammer (1997) and Chelton et al. (1998) used along-track TOPEX/Poseiden altimeter data to estimate global eddy spatial scales finding that eddy scales outside the tropics vary proportionally (though not identically) to the internal Rossby radius of deformation.

The Hawaiian Islands (Fig. 1) are located in the southern portion of the North Pacific Gyre in the presence of nearly persistent northeastward trade winds. The island chain has a significant effect on both ocean currents and winds (Xie et al., 2001). The mountain peaks on the islands of Maui and Hawai'i penetrate the trade wind inversion layer forcing the wind to flow around the islands creating a large wake region of weakened flow (Smith and Grubisic, 1993). An active and intense eddy field lies in the wake region, driven primarily by the wind stress curl and intrinsic instabilities in the ocean flow (Calil et al., 2008; Yoshida et al., 2010). Fig. 1 shows a map of eddy kinetic energy (EKE) from geostrophic currents (provided by AVISO) calculated from a combination of altimetry missions from 2000 through 2008. The effects of the islands on the ocean flow can be seen in the increase in EKE found leeward of the island chain.

With such dynamical variation, the Hawaiian Islands pose a difficult challenge to determine the dominant characteristics of oceanic variability. Understanding this variability is important for quantifying the circulation and it is also crucial for determining the decorrelation scales that are applicable for optimal interpolation, data assimilation, or state-estimation problems. In this paper, we present a robust method to determine the spatial variability that is applicable in both the horizontal and vertical. We apply the semivariogram method (Journel and Huijbregts, 1978; Kitanidis, 1997; Banerjee et al., 2004) to multiple years of satellite sea surface height (SSH) and temperature (SST) data along with *in situ* temperature and salinity profiles. Spectral analysis is also commonly used to compute spatial scales from

* Corresponding author.
E-mail address: dax@soest.hawaii.edu (D. Matthews).

0967-0637/$ - see front matter © 2011 Elsevier Ltd. All rights reserved.
doi:10.1016/j.dsr.2011.07.004

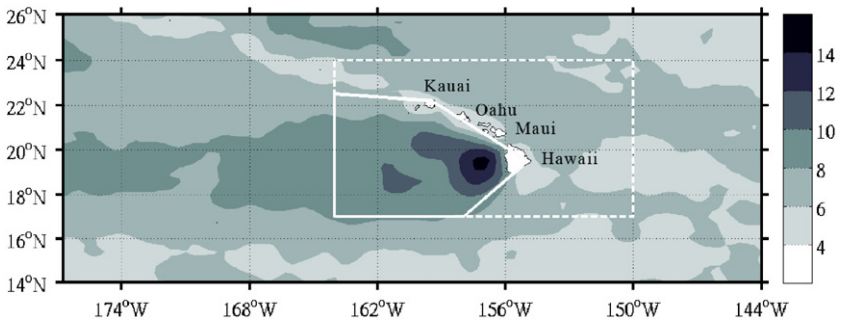

Fig. 1. The Hawaiian Islands, with leeward (solid white line) and windward (dot–dash white line) regions defined for semivariogram calculation. Contour levels show mean EKE levels for 2000 through 2008 from the AVISO absolute geostrophic velocity product.

oceanographic data, however it is not used because the method has problems with missing data and spectral slopes can be misinterpreted (Fasham, 1978). Geostatistical techniques, such as the semivariogram or the closely related autocorrelation method, proved less detailed information, but are more robust for geophysical data (Chelton and Schlax, 1991). The semivariogram method was chosen over the autocorrelation method to avoid using the "zerocrossing" of the autocorrelation function as a length scale estimate, which does not always exist. From the semivariogram we can also calculate the geophysical variability captured by the observations and the unresolved variance that provides an estimate of the measurement error. Because the eddy field dominates the variability of the ocean, we utilize anomaly data to limit the effect of large-scale mean dynamics in the statistics and to focus on the mesoscale. In Section 2, we present the semivariogram method and its application. In Sections 3 and 4, we present the results from the satellite and *in situ* data before concluding.

2. Concepts and definitions

Combining spatially and temporally sparse data to determine the variability characteristics (actual variability and the length scale of decorrelation) is a difficult challenge. The semivariogram function describes the covariance of sparsely distributed data as a function of distance (Banerjee et al., 2004), and has been used successfully for ocean dynamics (Seuront and Lagadeuc, 1997; Doney et al., 2003; Milliff et al., 2003; Powell et al., 2008).

The semivariogram is defined as

$$\gamma(h)=\tfrac{1}{2}E\left[(z(x+h)-z(x))^2\right], \tag{1}$$

where E is the linear expectation, h is the lag distance, $z(x)$ represents the data value at a given location, x, and $\gamma(h)$ is defined as the semivariogram function (the term variogram is used for $2\gamma(h)$). Thus, the semivariogram is the mean squared difference of all values within h distance of x. Because values are scattered spatially, no value of h is consistent, so a range of distances are used to bin the data: $h=h_o\pm\delta h$. These lag bins provide enough data such that the E operator is significant.

Data residuals are first computed for all available lag distances within the data and binned. Binning sizes were chosen to be as small as possible, while maintaining significant and consistent sample numbers per bin. Once computed, the set γ (Eq. (1)) is considered the empirical semivariogram composed only of observed data.

A statistical model is commonly fit to the computed empirical semivariogram for a mathematical representation of the variance (Journel and Huijbregts, 1978). This statistical model provides a tool for describing how a measurement varies as it is perturbed from its location. There are many mathematical models that may fit the semivariogram (exponential, circular, etc.), and after experimentation we found that a stationary Gaussian model (Kitanidis, 1997) most consistently represented the empirical semivariograms.

The Gaussian model:

$$\Gamma(h)=C_o+(\sigma^2-C_o)(1-\exp(-h^2/L^2)) \tag{2}$$

is fit to the empirical semivariogram, $\gamma(h)$, values using linear least-squares to solve for the model parameters C_o, σ^2, and L. The "nugget", Co, gives the zero-lagged or unresolved variance. The upper limit of the variance, σ^2, is called the "sill" and represents the value at which the data is no longer correlated. The lag distance, h, between C_o and σ^2 is estimated by L. Because the Gaussian function decays asymptotically, this "range" is estimated by (Kitanidis, 1997)

$$\alpha\approx 7L/4. \tag{3}$$

To generate the characteristics of the variability the observational data is used with predetermined lag bins to compute the empirical semivariogram. The modeled semivariogram is generated by fitting the Gaussian model (Eq. (2)) to the empirical semivariogram. From this fit, we generate our estimates of the unresolved variance (hereafter measurement error), C_o, and the maximum variance (hereafter variability), σ^2. The difference between the sill and the nugget is attributed to the geophysical variability captured by the observations. The length scale over which the geophysical variability is significant is the range, α. As the range is exceeded and the variance reaches σ^2, two observations are considered randomly correlated.

We now turn our attention to employ this semivariogram method on a variety of data to determine the measurement error, variability, and length scales around the Hawaiian Islands.

3. Horizontal variability and length scales

To analyze the horizontal variability and length scales around the Hawaiian Islands we use four years of satellite sea surface height and temperature data from 2004 through 2007. We chose this period because of the availability of satellite altimetry data. At least two satellites are required to map the ocean; however with additional satellites the resolution of SSH measurements is greatly enhanced (La Traon et al., 2001). During this time there are four satellite altimeters available, until the failure of Topex/Poseidon in 2006. While altimetry data is better suited to capture eddy size and fluctuations, SST has also been shown to be an indicator of eddy scale (Krause et al., 1990).

We analyze the along-track sea level anomaly product (SLA) produced by Ssalto/Duacs and distributed by AVISO (with support from CNES) from the altimeters onboard the TOPEX/Poseidon,

Jason-1, Envisat, and Geaosat Follow On (GFO) satellites. To generate SLAs, AVISO references sea surface height (SSH) data to a seven-year mean sea surface (MSS). The MSS corresponds to marine geoid undulations and to "permanent" sea level rise, and is computed using the CLS01_MSS statistical model from altimetric data (Dibarboure et al., 2009). SLA data are used instead of SSH to minimize the effects of large-scale dynamics in the semivariogram and to focus on the mesoscale eddy field. Along-track data are used in place of available gridded data because we do not wish to bias our length scale estimates with *a priori* specified scales that are used in the mapping procedure at AVISO (Dibarboure et al., 2009). The along-track data are at ~6 km spacing for TOPEX/Poseidon and Jason-1, ~7 km for Envisat, and ~10 km for GFO. The cross-track resolution varies depending on the satellites overhead and their current orbital path. Locations of the along-track data used are shown in Fig. 2.

SST data are taken from the daily, 4 km Pathfinder version 5 product provided by NASA's Physical Oceanography Distributed Active Archive Center. The Pathfinder product combines available infrared radiometry data from the advanced high-resolution radiometer (AVHRR) instruments onboard multiple satellites (Kilpatrick et al., 2001). We filter the data with the provided quality flags to keep only the highest quality data. A map of the number of SST data used is shown in Fig. 2. The increase in coverage in lee of the islands is due to the westerly reversal of the winds that keep the island wakes cool and nearly free of clouds during the day (Yang et al., 2008). This data set was chosen over microwave SST data because of the higher resolution and over interpolated IR (or microwave-IR) because of the imposed length scales in the gridding procedure.

Surface water temperatures in the region have a strong meridional gradient and a slight zonal gradient, with warmer in the southwest due to the Hawaiian Lee Counter Current (Lumpkin, 1998) and an annual cycle varying between an average of 23 °C in winter and 27 °C in summer. To focus on the mesoscale eddy field using SST data the spatial trends and a seasonal cycle must be removed from the data to generate anomalies (SSTA). No significant annual cycle was found in SSH data, so a seasonal signal was not removed from those data. In preliminary experiments, the seasonal cycle was computed from daily mean values, with the mean spatial field computed from the temporally detrended data. These two means were removed from the daily SST maps to produce SSTAs. We found that semivariograms using these data did not properly resolve the sill, as the variance continued to increase with the lag distance. A running seasonal mean of four months was found to best remove the seasonal spatial signal and produce stable, consistent semivariograms.

3.1. Regional semivariograms and results

We computed isotropic semivariograms within the windward and leeward regions shown in Fig. 1. Meridional and zonal semivariograms are also computed within each region to find any anisotropic variability or directional length scale differences. Empirical semivariograms were generated using 20 km lag bins, from a lag distance of 0–500 km, which maintained a minimum of 1700 observation residuals per bin. The average and minimum number of points per bin for each case is shown in Table 1.

Empirical semivariograms from both SLA and SSTA data show increased variability at shorter length scales in the lee of the

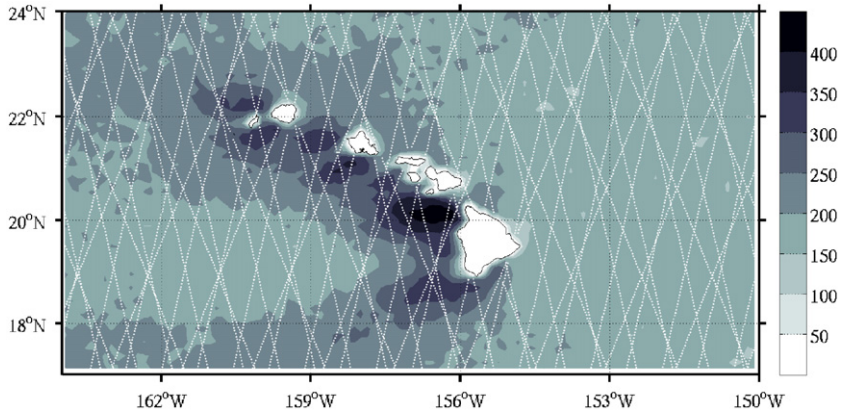

Fig. 2. Locations of SLA observations considered and contour of the number of SST observations used.

Table 1
Horizontal statistics from the Gaussian model fit to leeward and windward empirical semivariograms.

	SLA			SSTA		
	Isotropic	**Zonal**	**Meridional**	**Isotropic**	**Zonal**	**Meridional**
Windward						
Length-scale	224.13 km	224.39 km	255.25 km	245.97 km	223.50 km	285.87 km
Variability	0.0046 m^2	0.0046 m^2	0.0046 m^2	0.116 K^2	0.110 K^2	0.133 K^2
Meas. Error	6.83e−4 m^2	7.14e−4 m^2	6.7e−4 m^2	0.047 K^2	0.121 K^2	0.140 K^2
Mean #/bin	19,550	10,130	3350	70,140	38,500	11,880
Min #/bin	9120	5380	1730	31,440	16,180	6300
Leeward						
Length-scale	171.0 km	158.27 km	184.05 km	181.14 km	200.75 km	197.20 km
Variability	0.0066 m^2	0.0064 m^2	0.0066 m^2	0.127 K^2	0.121 K^2	0.140 K^2
Meas. Error	6.24e−4 m^2	5.78e−4 m^2	4.96e−4 m^2	0.051 K^2	0.058 K^2	0.060 K^2
Mean #/bin	132,510	19,600	25,430	291,920	52,440	43,150
Min #/bin	9640	1790	2190	26,370	4680	1870

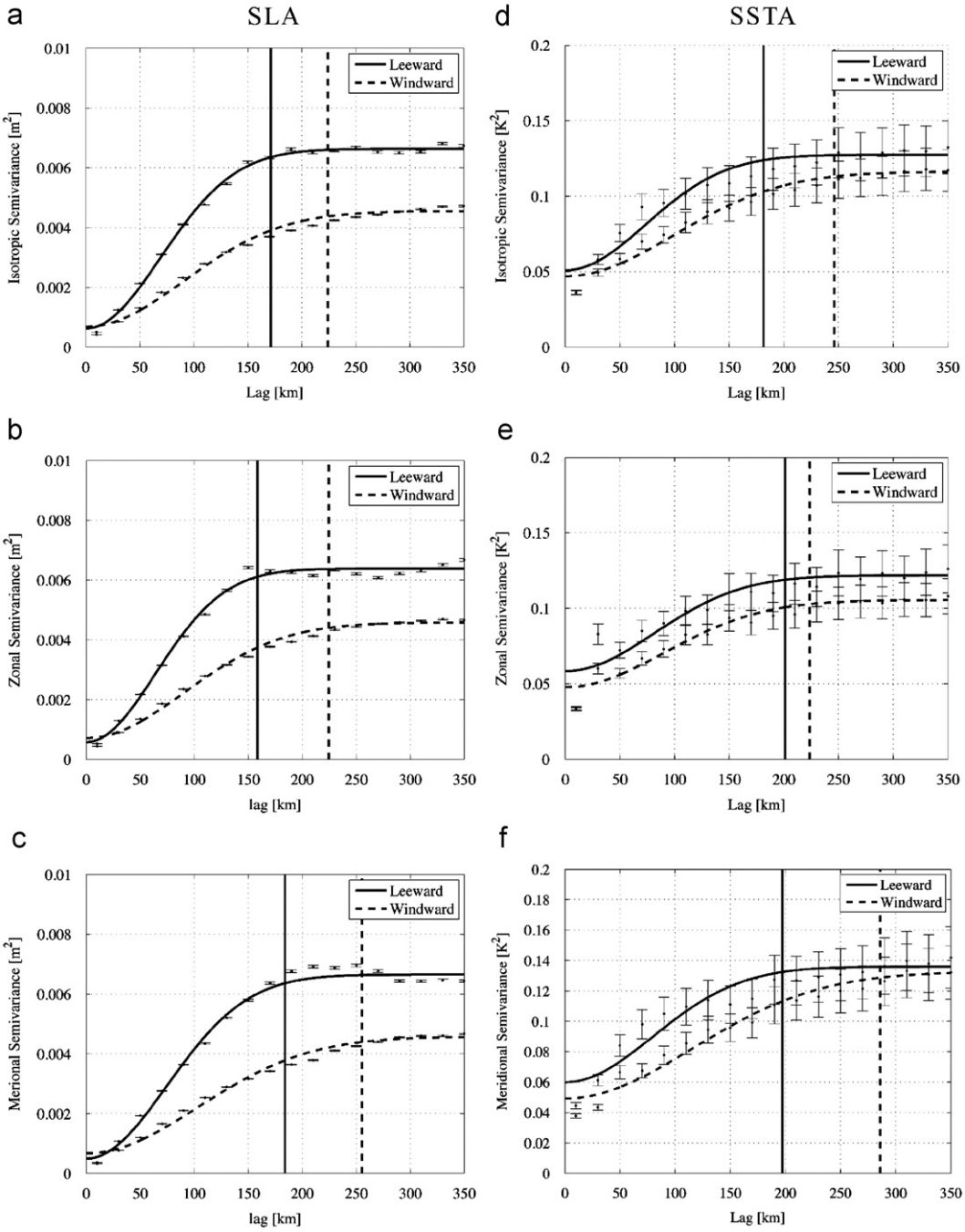

Fig. 3. Leeward and windward modeled (lines) and empirical (points with error bars) semivariograms for isotropic (a,d), meridional (b,e), and zonal cases (c,f) from SLA (a–c) and SSTA (d–f) data.

islands. The increase in SLA variability is expected as EKE has been shown to increase westward of the Island of Hawai'i (Qiu et al., 2008) and the difference in leeward and windward isotropic variability is far more pronounced in the SLA data compared to SSTA (Fig. 3a). From SSTA data higher leeward variability is found, however the differences in the leeward and windward isotropic variances are within the range of the standard deviation within each semivariogram bin (Fig. 3d).

The Gaussian model (Eq. (2)) fit to the empirical semivariogram provides the length scale, variability, and measurement error estimates shown in Table 1. The isotropic geophysical variance captured by the SLA observations is 50% greater in the leeward region, compared to 15% in SSTA observations. With length scales of 170 km and 225 km in the leeward and windward regions, a reduction of 55 km is found in the leeward SLA data (Fig. 3a). Length scales from SSTA data are on the same order to those from SLA data and show a similar isotropic reduction of 65 km in leeward length scale (Fig. 3d).

Stammer (1997) estimated eddy scales from TOPEX data as the lag distance of the first zero crossing of the autocorrelation function. For the Hawaiian Island region a length scale of approximately 150 km is found. The longer length scales estimated here are likely due to methods used. Autocorrelation functions applied to SLA data commonly show negative lobes due to the removal of the oceanic signal at large wavelengths (Le Traon and Minster, 1993). As a test, we computed the

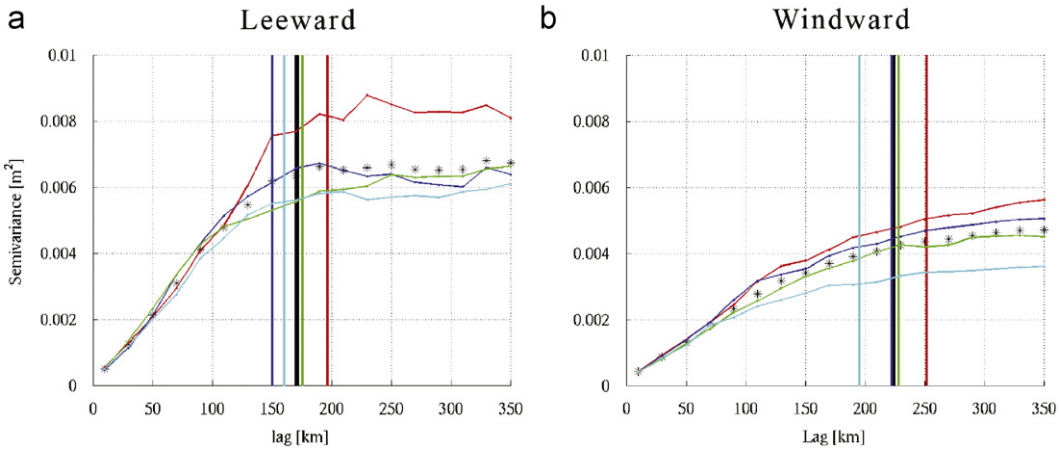

Fig. 4. Estimates of leeward (a) and windward (b) SLA semivariance (points) and length scale (vertical lines) from each of the 4 years used in the study along with the time average (black line and asterisks). Colors correspond to 2004 (red), 2005 (blue), 2006 (green), and 2007 (cyan). (For interpretation of the references to color in this figure legend, the reader is referred to the web version of this article).

autocorrelation function and found the first zero crossing was consistently shorter than the length scale estimated from the semivariogram method when a significant negative lobe existed.

Length scales were found to be anisotropic in the windward region, with meridional length scales 25 km longer than the zonal in SLA data and 60 km longer in SSTA (Table 1). The merdionally extended length scales are likely due to large-scale trends in the anomaly data that are tied to the latitudinal variation in SST and the North Pacific Gyre in SSH. In lee, where eddies dominate the flow and the islands disrupt the zonal SST pattern (Xie et al., 2001), meridonal and zonal length scales are closer in value, being almost identical in SSTA.

To examine the consistency of the length scale estimates we calculated the windward and leeward length scales for each of the four years used in the study. Fig. 4a and b shows the semivariograms from SLA data for each year along with the corresponding length scale. The standard deviations of the length scale estimates are 20 and 23 km for the leeward and windward regions, respectively. While there is a fair amount of variation between years, the windward region length scale was found to be consistently longer than the leeward, with the standard deviation of the differences between the regions being less than 15 km. The variation in length scale estimates from SSTA data is larger, with annual standard deviations of 44 km and 53 km for the leeward and windward regions, although, windward length scales are again found to be consistently longer.

The estimates of measurement error show little variation between the regions or directions, with values of 3.46 cm and 0.31 K for SLA and SSTA, respectively. The estimated error from the SLA semivariogram is higher than both the 3 cm instrument error found in Jason-1 (Ponte et al., 2006) and 1.7 cm in TOPEX/Poseiden SSH measurements (Leben and Powell, 2003), suggesting some unresolved variability at scales shorter than the first lag bin. The SSTA RMS compares favorably with the 0.3 K errors found in pathfinder SST observations (Kearns et al., 2000).

These results demonstrate that in lee of the island variability is increased and length scales are decreased, however estimates from SLA and SSTA data slightly vary. Differences in the statistics generated from the two products are due to a few reasons. The data sets are not coincident in time or space and features captured by one data set may not be in the other. It is also possible to have an eddy with little or no SST signature. Furthermore, temperature variance at the sea surface is not only a function mesoscale dynamics and may be produced by various processes. While the use of daily images with a seasonal mean field removed should enhance the signal of mesoscale features in SST imagery, it is likely that some large-scale signals persist in the SSTA data.

3.2. Spatial patterns

In the previous section, we compared the values over the two regions; however, we wish to understand the spatial distribution of horizontal variability and length scales around the islands. We computed semivariograms (Eq. (1)) for 1° boxes across the region using 20 km lag bins from 0 to 500 km. The modeled semivariograms (Eq. (2)) were fit to the empirical semivariogram bins containing more than 100 values to estimate the variability and length scales around the domain. This was the minimum number of data required to stabilize the semivariogram, though a data set with more noise or measurement error may require more values per bin. A region was not considered if the correlation coefficient between the empirical and modeled semivariograms had less than 99% statistical significance. To provide a clear picture of the variability and length scales we use a Laplacian diffuser to interpolate the values across the region.

To diffuse the values from 1° resolution to 0.1°, we repeatedly run the Laplacian diffusion, $\nabla^2\theta$, where θ is the field of interest until it has converged. That is, further diffusion leads to minimal changes in the field. This repeated integration is shown by

$$\theta(n+1) = \nabla^2\theta(n) + r\theta(0). \tag{4}$$

The new field, $\theta(n+1)$, is the result of the diffusion of the previous field, $\theta(n)$, plus a term to maintain the original 1° values, $\theta(0)$. The factor r is given by

$$r = \begin{cases} 1 & \text{if} \quad \theta_{ij}(n) \le \theta_{ij}(0) - \varepsilon \\ 0 & otherwise \end{cases} \tag{5}$$

where $\varepsilon = stdev(\theta(0))/100$. This allows us to downscale the 1° data in a Gaussian manner without imposing interpolation length scales.

In general, local values agree with those from the leeward and windward estimates in the previous section. Total variability is higher in lee of the islands (Fig. 5b and d) with reduced length scales (Fig. 5a and c). The largest SLA variability is found directly in lee of the island and northwest of the island chain. The increase in variability in the northwest is not attributed to the islands, but instabilities in the mean flow associated with the subtropical gyre (Chen and Qiu, 2010). Total variability in SSTA observations is found to be highest northwest of the islands, also with increased

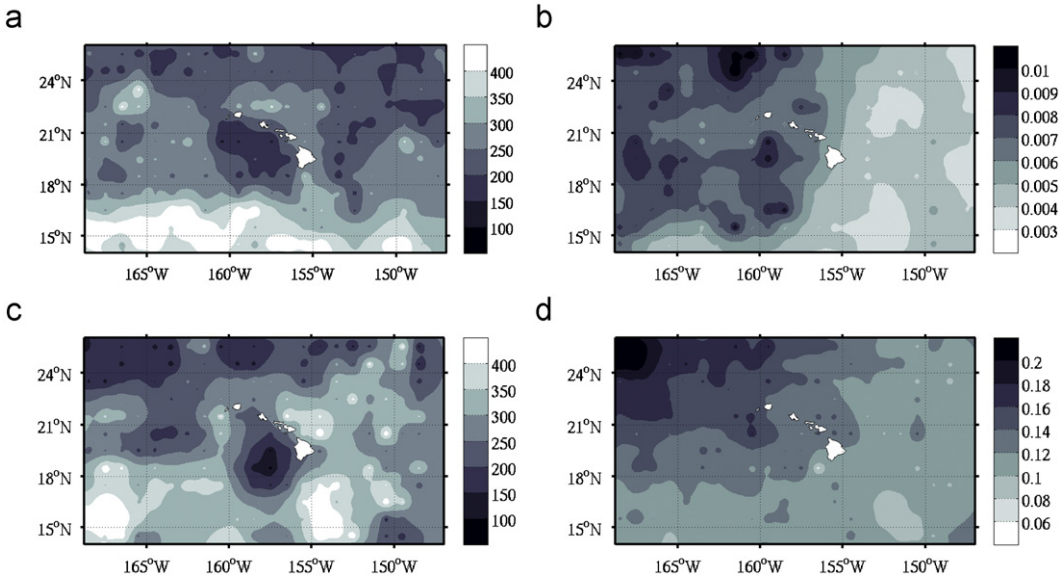

Fig. 5. Contour plots of the diffusion of $1^\circ \times 1^\circ$ estimates of length scale [km] (a,c) and variance (b,d) from SLA [m^2] (a,b) and SSTA [K^2] data (c,d).

variability directly leeward of the islands. The high SSTA variability northwest of the islands is connected to a basin scale pattern in variance associated with anomalies in zonal wind stress (Yeh and Kirtman, 2004). In lee of the islands, the high SSTA variability that extends to the western edge (Fig. 5d) is due to both the warm waters of the HLCC (Xie et al., 2001) and the increased eddy activity in lee of the islands.

Previous results from altimetry have shown a clear latitudinal variation of length scale, decreasing toward the poles (Le Traon et al., 1990). Length scale estimates shown in Fig. 4a and c demonstrate a meridional gradient higher than previously reported, with length scales ~200 km at 26° and ~300 km at 14°N. The results are more similar to the variation in Rossby radius, which has a much stronger gradient at lower latitudes (Chelton et al., 1998). The effects of the islands on the length scale are clearly seen by the reduction found directly in the lee of the Island of Hawai'i where strong eddies form. In a large area from the Island of Hawai'i to 160°W and from the Island of Kaua'i to 18°N, SLA length scales are 50 km shorter than directly windward of the islands. The shortest length scales found in this region coincide with the highest variability, around 400 km west of the Island of Hawai'i and directly south of Kauai. West of this area an abrupt change in the zonal gradient of length scale is found, with length scales increasing by over 75 km at 160°W. There are two possible processes related to the observed increase in length scale west of 160°W. As eddies in lee of the islands move downstream they coalesce and merge, causing abrupt changes in length scale (Flament et al., 2001a), and it is possible that such a transition commonly occurs here. Also, by analyzing the eddy variability separated into two geographical regions, the immediate lee southwest of Hawai'i and westward of 160°W along 19°N, Yoshida et al. (2010) demonstrated that these regions were dominated by differing temporal signals. In the immediate lee eddy variability was dominated by 60-day signals that were related to wind stress curl variability. Westward of 160°W variability was dominated by 100-day signals that were likely linked to instabilities in the shear between the North Equatorial Current and the Hawai'i Lee Counter Current. These forcing mechanisms that are dominated by varying temporal signals likely generate eddy variability with different length scales. It is plausible that both of these processes are related to the increase in length scale observed.

Fig. 5c and d shows a similar reduction of length scale from SLA and SSTA data; however, from SSTA data the reduction is much more defined in the wake region behind the Island of Hawai'i. In this area there is poor altimetry coverage, with only one ascending and one descending pass (Fig. 2), and may explain why the further reduction in length scale seen in the SSTA map is not captured by SLA data.

The relation between the spatial scale and internal Rossby radius is given by the ratio of EKE to eddy potential energy for quasi-geostrophic motions (Pedlosky, 1979). The similarity in leeward patterns of mean EKE and length scales suggests that the immediate lee of the Island of Hawai'i is the primary area of transfer of eddy energy from potential to kinetic, as this is the region where the dominant length scales vary most from the internal Rossby radius.

4. Vertical variability and length scales

In the lee of the islands, blockage of the wind leads to an increase in eddy variability though Ekman pumping and through baroclinic instabilities in the mean wind-driven flows (Calil et al., 2008). These processes will impact the vertical variability and length scale. Using all available *in situ* data, we compare the vertical characteristics of the variability in the immediate lee of the islands with the abyssal region around the islands.

Because of the relative lack of *in situ* data (as compared to satellite data), a greater temporal range of data was utilized. The analysis used Argo data from 2002 through 2009, Seaglider data from 2008 through 2009, and ship-borne profile data from 1988 through 2009. The Argo program is a global array of vertical profiling floats that provide temperature and salinity profiles every 10 days at depths ranging from the surface to 2000 m. On average, Argo floats have 3° horizontal and 10 m vertical resolution. The University of Hawai'i operates a number of autonomous, buoyancy driven Seagliders in the region that are capable of directed missions and can sample temperature and salinity from the surface to 1000 m. Data were collected from several glider missions as part of the Hawai'i Ocean Time-series (HOT) program and Hawai'i Ocean Observing System (HiOOS) primarily around the Island of Oahu. Due to the nature of the Seaglider motion, horizontal and vertical resolutions are variable. We also utilize

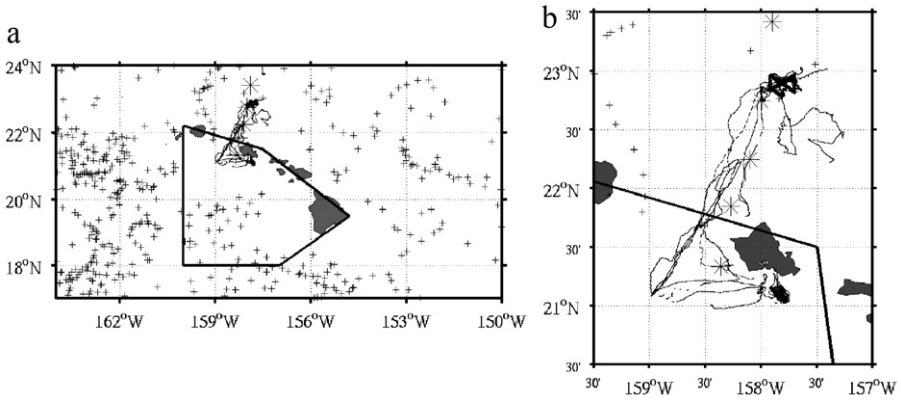

Fig. 6. (a) Locations of *in situ* measurements found in the Immediate lee (inside black box) and abyssal (outside box) regions; (b) a closer view of the locations of data from around the Island of Oahu.

temperature and salinity profile data from HOT cruises, which provide monthly repeated observations from both ship and mooring. The horizontal distribution of the hydrographic observations is shown in Fig. 6a, with a closer view of the observations around the Island of Oahu in Fig. 6b. From these platforms there are over 11×10^6 temperature and salinity observations available, from which 50% are from Seagliders, 49% from HOT cruises, and 1% from Argo. We will combine the data from two regions: immediate lee and abyssal (Fig. 6).

Below the mixed layer, temperatures drop from 25 °C near the surface to less than 5 °C below 1000 m. Salinity levels peak above 35 near 100 m depth due to higher salinity surface water mixed from the north. Lower salinity waters at 500 m depth are traceable to fresher surface water in the northwest. Below 500 m, salinity increases gradually with depth (Flament et al., 2001b). These mean profiles are removed from the data before semivariogram calculation to create both temperature and salinity anomalies consistent with Section 3. Vertical empirical semivariograms are generated for all data within each region using 5 m lag bins from a lag distance of 0–500 m.

In the immediate lee, the temperature variability is double that in the abyssal region, with vertical length scales 40 m longer (Table 2 and Fig. 7a and b). This regional difference in variability is not found in the salinity observations; however, the vertical length scale from salinity data is 25 m longer in the immediate lee. The majority of data used in the immediate lee was from glider missions around Oahu. In the lee, the island generates a wake of reduced winds, which result in decreased cloud cover and increased water temperature. South of Oahu strong winds flow between Molokai–Lanai–Maui and Oahu (Yang et al., 2008), yielding cooler waters. Resulting wind shear on the edge of the wake causes convergence of the Ekman transport (Chevanne et al., 2002; Jiménez et al., 2008), bringing together warm waters from the wake region with the relatively colder well stirred water from the unsheltered region. The mixing of the different temperature waters by convergence due to Ekman transport and eddies generated in lee of the islands are the likely causes of the increase in temperature variability observed. Also, convergent currents would lead to a depressed thermocline, which is a possible explanation of the longer vertical scales seen in the immediate lee.

If atmospheric processes were the cause of these regional variations in vertical variability and length scales the effects would be most apparent in shallow waters. We computed shallow-water semivariograms from temperature data for 40 m vertical sections from the surface to 300 m (Fig. 8). Vertical temperature variability is found to be larger in the immediate lee at all depths; however, the variance is doubled in waters shallower than 140 m. It is in these shallower depths that temperature vertical length scales are significantly increased.

Table 2
Vertical statistics from the Gaussian model fit to temperature and salinity empirical semivariograms.

	Temperature		Salinity
Windward			
Length-scale	93.17 m		106.57 m
Variability	0.43 K^2		0.009
Meas. Error	0.073 K^2		7.36e−4
Mean #/bin		590,416	
Min #/bin		283,360	
Leeward			
Length-scale	132.50 m		133.84 m
Variability	1.02 K^2		0.011
Meas. Error	0.07 K^2		0.0013
Mean #/bin		90,440	
Min #/bin		7506	

The statistics presented in this section are from data primarily around the Island of Oahu. However, these results should be representative of the processes that occur in lee of each island in the Hawaiian Archipelago.

Estimates of temperature measurement error were 0.37 K for both regions, which is slightly higher than the value estimated from satellite observations. Salinity estimates of measurement error were 0.044 for both regions. Both estimates are well above the stated instrument errors of the CTD packages used on Seagliders, ARGO floats, and HOT cruises, of which, ARGO is the least accurate (0.005 K and 0.01, for temperature and salinity, respectively; Oka and Ando, 2006). This suggests that unresolved variance remains at the shortest lag, within the 5 m bin.

5. Conclusions

The Hawaiian Islands significantly alter the variability and length scales of the ocean. On average, SLA observations exhibit a 50% increase in variability in lee of the islands, at a length scale that is 55 km shorter than the windward side. A consistent reduction in leeward length scale was found in each of the four years studied, suggesting this pattern would be found if these computations were applied to data in different years. While increased variability in SSH and increased EKE are known to persist for over 1000 km westward of the islands (Qiu et al., 2008), the effect of the islands in reducing horizontal length scales is focused in the lee, 300–400 km west of the Island of

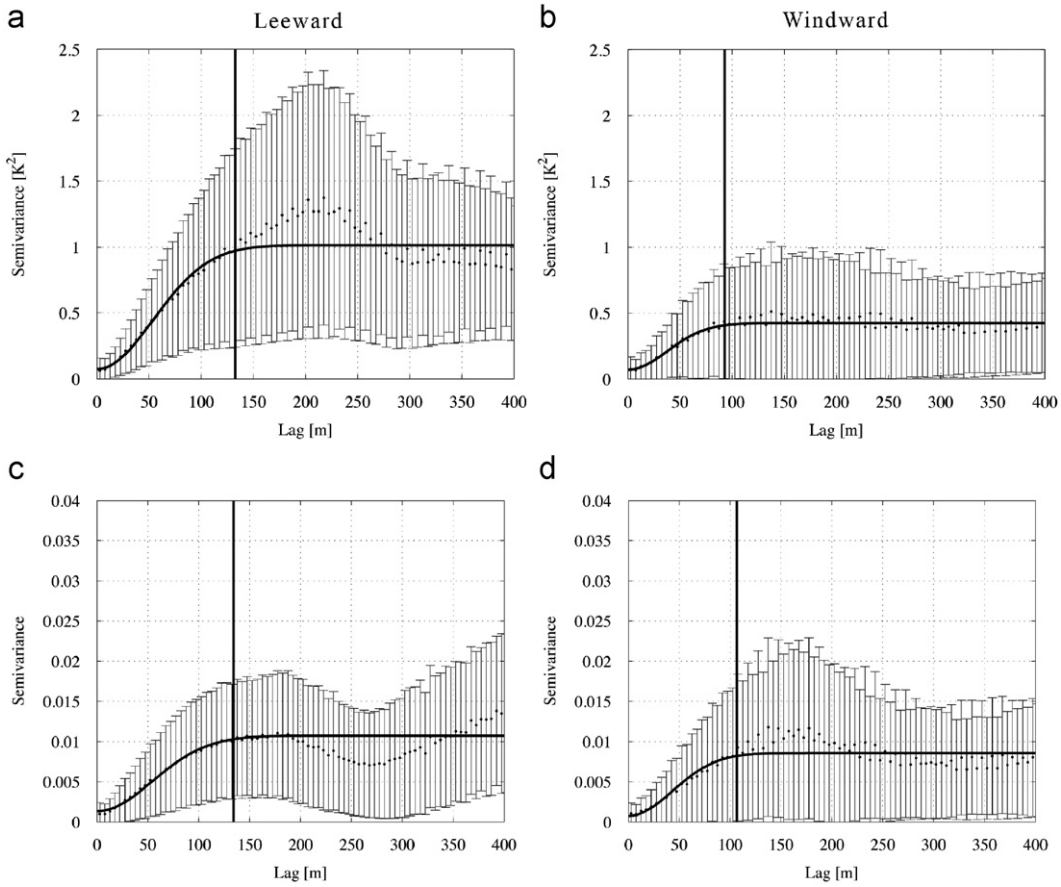

Fig. 7. Immediate lee (a and c) and Abyssal (b and d) semivariograms for temperature and salinity data.

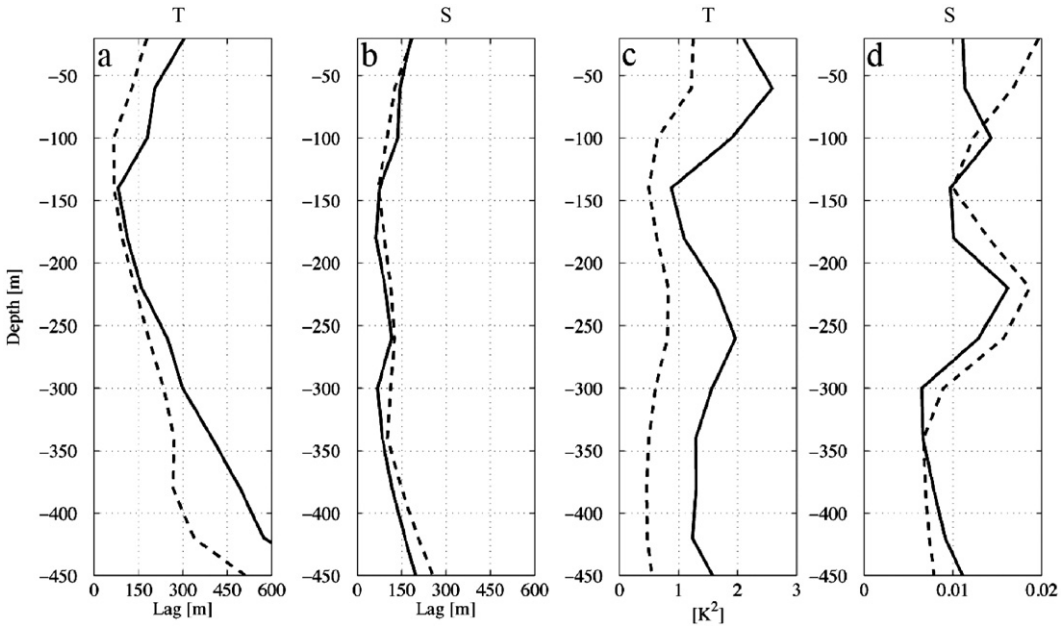

Fig. 8. Length Scale and variability estimates as a function of depth from temperature data (lee region is shown by the solid line, while the abyssal region is the dashed).

Hawai'i. A transition to longer length scales west of 160° W is likely due to the merging of eddies as they propagate westward and a change in the generation mechanism for eddy variability. Where horizontal length scales are reduced, vertical length scales are increased by 30 m on average and vertical temperature variability is doubled. This increase in variability and increased length scales are found primarily above 140 m depth and are linked an oceanic response to atmospheric conditions.

These statistical length scales provide a robust measure of the decorrelation lengths for data in the Hawaiian region for use in optimal interpolation or data assimilation schemes. We intend to use these values, and their spatial variation, for assimilating data

in the Hawaiian region following Powell et al. (2008); however they are also well suited for other data blending methods. Also, while not presented here this methodology has the potential to be applied to identify the dominant temporal scales of eddy variability in different regions. Although, because of the time between repeat altimetry passes (10–35 days) SLA data would not be ideal for time scale estimation, however a daily gridded product such as Pathfinder would work well.

Acknowledgments

Dr. Matthews was support by NOAA Grant # NA07NOS4730207 and Dr. Powell was support by The Office of Naval Research Grant # N00014-09-10939. The authors would also like to thank Prof. Glenn Cater for providing Seaglider observational data and Prof. Roger Lukas for providing Hawai'i Ocean Time-series observations, which are supported by the U.S. National Science Foundation under Grant OCE-0327513. This is SOEST publication no. 8376.

References

Banerjee, S., Carlin, B., Gelfand, A., 2004. Hierarchical Modeling and Analysis for Spatial Data, Monographs on Statistics and Applied Probability 101. Chapman and Hall/CRC Press, Boca Raton, FL 451 pp.

Calil, P.H., Richards, K., Jia, Y., Bidigare, R., 2008. Eddy activity in the lee of the Hawaiian Isands. Deep Sea Res. II 55, 1179–1194.

Chelton, D.B., Schlax, M., 1991. Estimation of time averages from irregularly spaced observations: with application to Coastal Zone Color Scanner estimates of chlorophyll concentration. J. Geophys. Res. 96, 14 669–14 692.

Chelton, D.B, de Szoeke, R., Schlax, M., Naggar, K., Siwertz, N., 1998. Geographic variability of the first baroclinic Rossby radius of deformation. J. Phys. Oceanogr. 28, 433–460.

Chen, S., Qiu, B., 2010. Mesoscale eddies northeast of the Hawaiian archpelago from satellite altimeter observations. J. Geophys. Res. 115, C03016.

Chevanne, C., Flament, P., Lumpkin, R., Dousset, B., Bentamy, A., 2002. Scatterometer observations of wind variations induced by ocean islands: implications for wind-driven ocean circulations. J. Remote Sensing 28 (3), 466–474.

Danztler Jr., H.L., 1977. Potential energy maxima in the tropical and subtropical North Atlantic. J. Phys. Oceanogr. 7, 512–519.

Dibarboure, G., Lauret, O., Mertz, F., Rosmorduc, V., Maheu, C., 2009. SSALTO/DUACS User Handbook: (M)SLA and (M)ADT Near-Real Time and Delayed Products. CLS-DOS-NT-06.034 Iss:2.1.

Doney, S.C., Glover, D., McCue, S., Fuentes, M., 2003. Mesoscale variability of Sea-viewing Wide Field-of-view Sensor satellite ocean color: global patterns and spatial scales. J. Geophys. Res. 108 (C2).

Fasham, M.,1978. The application of some stochastic processes to the study of plankton patchiness. In: Oceanography and Marine Biology: An Annual Review, vol. 16, pp. 43–79.

Flament, P., Lumpkin, R., Tournadre, J., Armi, L., 2001a. Vortex pairing in an unstable anticyclonic shear flow: discrete subharmonics of one pendulum day. J. Fluid Mech. 440, 401–409.

Flament, P., Kennan, S., Lumpkin, R., Sawyer, M., Stroup, E., 2001b. The Ocean Atlas of Hawai'i. University of Hawai'i Press, Honolulu, Hawai'i.

Jiménez, B., Sangrà, P., Mason, E., 2008. A numerical study of the relative importance of wind and topographic forcing on oceanic eddies shedding by deep water islands. Ocean Modelling 22, 146–157.

Journel, A.G., Huijbregts, C., 1978. Mining Geostatistics. Acedemic Press, Harcourt Brace Jovanovich Pubilshers, New York, New York 600 pp.

Kearns, E., Hanafin, J., Evans, R., Minnett, P., Brown, O., 2000. An independent assessment of Pathfinder AVHRR sea surface temperature accuracy using the marine atmosphere emitted radiance interferometer (MAERI). Bull. Am. Meteorol. Soc. 81, 1525–1535.

Kilpatrick, K.A., Podesta, G., Evans, R., 2001. Overview of the NOAA/NASA advanced very high resolution radiometer pathfinder algorithm for sea surface temperature and associated matchup database. J. Geophys. Res.—Oceans 106 (C5), 9179–9197 MAY 15 2001.

Kitanidis, P.K., 1997. Introduction to Geostatistics, Applications in Hydrogeology. Cambridge University Press, New York, New York 249 pp.

Krause, W., Doscher, R., Lehmann, A., Viehoff, T., 1990. On eddy scales in the eastern and northern Atlantic Ocean as a function of latitude. J. Geophys. Res. 95, 18 049–18 056.

La Traon, P.Y., Dibarboure, G., Ducet, N., 2001. Use of a high-resolution model to analyze the mapping capabilities of multiple-altimeter missions. J. Atmos. Oceanic Technol. 18, 1277–1288.

Leben, R.R., Powell, B., 2003. Accuracy assessment of Jason-1 and TOPEX/POSEIDON along-track sea surface slope. Marine Geodesy 26 (3–4), 355–366.

Lee, D.K., Niiler, P., 1987. The local baroclinic instability of geostrophic spirals in the eastern North Pacific. J. Phys. Oceanogr. 17, 1366–1377.

Le Traon, P.Y., Rouquet, M., Boissier, C., 1990. Spatial scales of mesoscale variability in the North Atlantic as deduced from Geosat data. J. Geophys. Res. 95 (C11), 20267–20,285.

Le Traon, P.Y., Minster, J., 1993. Sea level variability in the South Atlantic subtropical gyre: semi-annual Rossby waves and large scale signal. J. Geophys. Res. 98, 12315–12326.

Lumpkin, C.F., 1998. Eddies and Currents in the Hawaiian Islands. Ph.D. Thesis. SOEST-School of Ocean and Earth Science and Technology, University of Hawai'i at Manoa, 282 pp.

Mercier, H., Colin de Verdiere, A., 1985. Space and time scales of mesoscale motions in the eastern North Atlantic. J. Phys. Oceanogr. 15, 171–183.

Milliff, R.F., Niiler, P., Morzel, J., Sybrandy, A., Nychka, D., Large, W., 2003. Mesoscale correlation length scales from NSCAT and Minimet surface wind retrievals in the Labrador Sea. J. Atmos. Oceanic Technol. 20, 513–533.

Oka, E., Ando, K., 2006. Stability of temperature and conductivity sensors of Argo profiling floats. J. Oceanogr. 60, 253–258.

Pedlosky, J., 1979. Geophysical fluid dynamics. Springer-Verlag, New York.

Ponte, R.M., Wunsch, C., Stammer, D., 2006. Spatial mapping of time-variable errors in Jason-1 and TOPEX/Poseidon sea surface height measurements. J. Atmos. Ocean. Technol. 24, 1078–1085.

Powell, B.S., Arango, H., Moore, A., Di Lorenzon, E., Milliff, R., Foley, D., 2008. 4DVAR data assimilation in the Intra-America Sea with the Regional Ocean Modeling System (ROMS). Ocean Modeling 25, 173–188.

Qiu, B., Scott, R., Chen, S., 2008. Length scales of eddy generation and non-linear evolution of the seasonally modulated South Pacific Subtropical Countercurrent. Am. Meteor. Soc. 28, 1115–1528.

Richman, J.G., Wunsch, C., Hogg, N., 1977. Space and time scales and mesoscale motions in the sea. Rev. Geophys. 15, 385–420.

Seuront, L., Lagadeuc, T., 1997. Characterization of space-time variability in stratified and mixed coastal waters: application of fractal theory. Mar. Ecol. Prog. Ser. 159, 81–95.

Smith, R.B., Grubisic, V., 1993. Aerial observations of Hawaii's wake. J. Atmos. Sci. 50, 3728–3750.

Stammer, D., 1997. Global characteristics of ocean variability estimated from regional TOPEX/Poseidon altimeter measurements. J. Phys. Oceanogr 27, 1743–1769.

Wyrtki, K., Magaard, L., Hager, J., 1976. Eddy energy in the oceans. J. Geophys. Res. 81, 2641–2646.

Xie, S.P., Liu, W., Liu, Q., Nonaka, M., 2001. Far-reaching effects of the Hawaiian Islands on the Pacific Ocean–atmosphere system. Science 292, 2057–2060.

Yang, Y., Xie, S., Hafner., J., 2008. Cloud patterns lee of Hawaii Island: a synthesis of satellite observations and numerical simulation. J. Geophys. Res. 113, D15126. doi:10.1029/2008JD009889.

Yeh, S.W., Kirtman, B., 2004. The impact of internal atmospheric variability on the North Pacific SST variability. Clim. Dyn. 22, 721–732.

Yoshida, S., Qiu, B., Hacker, P., 2010. Windgenerated eddy characteristics in the lee of the Island of Hawaii. J. Geophys. Res. 115, C03019. doi:10.1029/2009JC005417.